

A novel dual thin-layer flow cell double-disk electrode design for kinetic studies on supported catalysts under controlled mass-transport conditions

Z. Jusys, J. Kaiser, R.J. Behm*

Department of Surface Chemistry and Catalysis, University of Ulm, D-89069 Ulm, Germany

Received 26 May 2003; received in revised form 6 August 2003; accepted 22 September 2003

Abstract

We present a novel dual thin-layer flow cell double-disk electrode design, which due to its high collection efficiency in combination with a reasonable time resolution allows highly sensitive measurements of electro-active species generated during electrochemical reactions on the working electrode. Most important, it allows for rapid changes of the electrolyte during the measurements, which in combination with a thin-film electrode, where an inert glassy carbon substrate is covered by a thin film of carbon-supported noble metal catalyst, makes it particularly useful for kinetic studies on electrocatalytic fuel cell reactions under realistic conditions (continuous reaction, continuous electrolyte flow) and on realistic materials (supported catalysts).

The performance of the set-up and its suitability for kinetic studies, in particular for transient experiments involving rapid electrolyte exchange, are demonstrated in potentiodynamic and transient potentiostatic measurements for the oxygen reduction reaction on carbon-supported Pt catalysts and, for comparison, on Pt-free Vulcan carbon supports.

© 2003 Elsevier Ltd. All rights reserved.

Keywords: Electrocatalysis; Flow cell; Thin layer cell; Supported Pt catalyst; Oxygen reduction; H₂O₂ formation

1. Introduction

Kinetic and mechanistic model studies of many electrocatalytic reactions depend crucially on a controlled mass transport to the electrode. This is particularly true for reactions involving dissolved gaseous species such as H₂ oxidation or O₂ reduction etc., because of the low concentrations of the reactants in the millimolar range. One important example is model studies on fuel cell (FC) reactions, which should be performed under conditions typical for fuel cell operation (continuous reaction, continuous mass transport, elevated temperatures, realistic catalysts) in order to yield results relevant for FC applications. This is most commonly achieved using the rotating disk electrode (RDE) technique [1–4]. Reactive reaction intermediates and reaction products generated during an electrocatalytic reaction can be determined in these experiments in a rotating ring-disk electrode (RRDE) set-up [5]. Due to a well-defined laminar flux of electrolyte over the ring-disk electrode assembly this allows to detect

the species formed on the rotating disk electrode at the surrounding ring electrode, which is set at such a potential that the reaction intermediates can be reduced (or oxidized) without interference with other electrochemical reactions. A typical example is the detection of H₂O₂ formed during O₂ reduction on the disk electrode by subsequent oxidation of the H₂O₂ to O₂ on the ring at potentials where other reactions such as anodic O₂ evolution can be ruled out [6].

Other hydrodynamic techniques available in electrochemistry, which have been extensively applied and described theoretically, include the Wall-Jet (or Impinging-Jet) disk electrode (WJDE) technique [7–11] and the (channel) flow cell technique [10–12]. In the WJDE design a continuous flow of electrolyte impinging at the static electrode surface results in a laminar flow of electrolyte at the electrode surface under certain conditions (flow rate, diameter of the inlet capillary and the electrode, nozzle-to-electrode distance), in contrast to the dynamic (rotating) electrode in the RDE configuration. In contrast to the R(R)DE technique, however, both the WJDE and the (channel) flow cell method were rarely used for studying electrocatalytic processes. The few examples for electrocatalytic WJDE studies

* Corresponding author.

E-mail address: juergen.behm@chemie.uni-ulm.de (R.J. Behm).

include CO oxidation on Pt electrodes [13–15] and studies on the effect of CO on H₂ oxidation [16]. The thin-layer flow cell technique was applied recently for methanol oxidation studies at elevated temperatures on Pt/Vulcan [17] and Pt-Ru electrodes [18].

In both techniques reactive products/intermediates can be detected via a second (detector) ring-shaped electrode or via a second stationary electrode (detector) placed in the flow channel downstream [19], which was used for various electro-analytical applications (see [12,20,21] and references therein). Being an open (flow-through) system and due to a rapid exchange of electrolyte at the electrodes combined with high collection efficiency, dual electrode channel flow cells are advantageous for transient kinetic measurements, which was equally demonstrated for numerous electro-analytical applications [12]. However, to the best of our knowledge, this hydrodynamic technique has not been applied so far for studying electrocatalytic reactions related to low temperature fuel cells, specifically, oxygen reduction reaction pathways.

The RRDE and WJDRE set-ups have the advantage of a rather short time required for the reactive species to be transported from the disk electrode (generator) to the ring electrode ('response time'), but may suffer from moderate collection efficiencies. Furthermore, RRDE does not allow fast electrolyte exchange under well-controlled conditions, which can become important, e.g., for studies of reactions on sensitive electrode surfaces. This can be accomplished in other channel flow designs such as the dual-band electrode [12,22] or the radial thin-layer ring-disk configuration [23], which can reach rather high (close to 100%) collection efficiencies at flow rates of submicroliter per second. At high collection efficiencies these designs suffer, however, from the generally very long times (minutes range) required for electrolyte transport from the first 'generator' electrode to the second one ('collector'). The resulting low time resolution makes them less suitable for kinetic studies.

In the present communication we report on a novel design of a dual thin-layer flow cell with a double-disk electrode (DTLFC-DDE), which is based on the dual thin-layer flow cell developed originally by Jusys et al. [24] for simultaneous differential electrochemical mass spectrometry (DEMS) and electrochemical quartz microbalance (EQM) measurements and applied later by Jusys et al. for DEMS measurements on supported catalysts ([25] and references therein), which combines a high collection efficiency and reasonable time resolution of the order of a few seconds. This set-up allows rapid changes from one electrolyte to another one under well-controlled conditions, which is typical for thin-layer cells due to their small volume in the microliter range [26], and therefore is perfectly suited for kinetic studies involving electrolyte exchange, as required, e.g. for transient studies of the removal of a pre-adsorbed adlayer. Furthermore, this approach compares favorably to the RRDE because of the high product collection efficiency at the collector [22,23], which will turn out to be ca. 80%

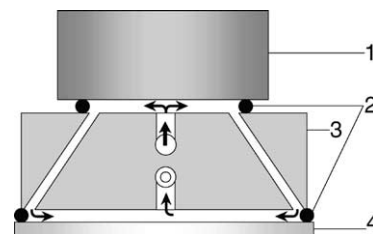


Fig. 1. Schematic drawing of the dual thin-layer double-disk electrode flow cell design, showing the glassy carbon substrate with the supported catalyst thin film at its inner side ('generator') (1), the Kalrez gaskets (2), the Kel-F body of the cell with the flow channels (3), and the second polycrystalline Pt electrode ('collector') (4).

in our configuration compared to typically about 20% in the RRDE configuration. The sensitivity for detection of electro-active products is increased accordingly.

In the following we will first, after a brief description of the DTLFC-DDE set-up and experimental details, characterize this set-up by cyclic voltammetry and calibrate it versus a Fe(III)/Fe(II) couple. In another part we will demonstrate the advantages and limitations of the approach compared to a standard RRDE configuration for the quantitative evaluation of the ORR pathways on Pt/Vulcan fuel cell catalyst. We will show that because of the advantages described above—small electrolyte volume, fast electrolyte exchange under controlled conditions, and high collection efficiency—the DTLFC-DDE approach introduced here is a highly advantageous electro-analytical tool for mechanistic and kinetic studies of electrocatalytic reactions under well-controlled conditions, both on massive model electrodes and state-of-the-art supported catalysts. This makes it particularly well suited for studies of electrocatalytic reactions under polymer electrolyte fuel cell relevant conditions and on fuel cell relevant materials.

2. Experimental

2.1. Dual thin-layer double-disk electrode flow cell

The experiments were performed in the dual thin-layer flow cell used for DEMS studies in previous publications (see [25] and references therein), which is based on the dual thin-layer flow cell design described in [24], modified correspondingly for the present electrochemical measurements (see Fig. 1). The cell itself consists of a circular Kel-F plate (5-mm thick) with capillaries for the electrolyte inlet and outlet, whose openings are centered on the opposite sides of the Kel-F plate. The connection between both compartments is made by four connecting capillaries positioned at the inner edge of two Kalrez gaskets (ca. 50- μ m thick), against which the working electrode or 'generator', a mirror-polished glassy carbon disk 9 mm in diameter with a 6-mm diameter thin Pt/Vulcan film, and the 'collector', a mirror-polished polycrystalline Pt disk 15 mm in diameter, exposed area 1.33 cm², were pressed to form two interconnected thin-layer compartments.

The incoming electrolyte first hits the center of the working electrode and spreads over its surface in the first thin-layer compartment, until it reaches the four outlet capillaries. During the residence time at the electrode the electro-active species can react and the reaction products are accumulated within the small electrolyte volume in the first compartment (ca. 5 μl), resulting in significant reaction-induced changes in the concentration of both educt and product. In the second thin-layer compartment the electro-active species can react at the second electrode, which is biased to a potential suitable for oxidation/reduction of these species. The electrolyte leaves the second thin-layer compartment through the outlet capillary positioned in the center of the opposite Kel-F wall. This way the dual thin-layer cell operates as a continuous flow-through reactor, with the supporting electrolyte serving as a carrier for both reacting species and products. A quantitative characterization of the electrochemical properties of the set-up will be presented in Section 3.1.

2.2. Further experimental details

The thin-film electrode was prepared as described previously [27]. In short, an aliquot of an aqueous suspension of the conditioned Pt/Vulcan catalyst (E-TEK, 20 wt.% Pt, conditioning 30 min in 10% O_2 in N_2 at 300 $^\circ\text{C}$, 30 min in H_2 at 300 $^\circ\text{C}$, at a gas flow rate 60 Nml/min and 30 Nml/min, respectively, atmospheric pressure) was pipetted onto a glassy carbon disk (Sigradur G, Hochtemperatur Werkstoffe), dried and fixed by a thin (ca. 0.1 μm) Nafion film, which was prepared by pipetting Nafion solution on top of the dried catalyst layer. The geometric area of the electrode is 0.28 cm^2 , the Pt loading 28 $\mu\text{g cm}^{-2}$. The average particle size and the particle size distribution of the Pt/Vulcan catalyst had been characterized recently by X-ray diffraction (XRD) and transmission electron microscopy (TEM), yielding an average particle size of 3.7 nm for the conditioned catalyst and a dispersion of 26% [28].

Two Pt wires connected through separate ports at the inlet and outlet of the cell served as counter electrodes. The reference electrode (saturated calomel electrode, SCE) was connected through a Teflon capillary at the outlet of the cell (all potentials are quoted versus that of the reversible hydrogen electrode (RHE)). The potentials of both generator and collector were controlled using a standard bi-potentiostat from Pine Instruments. The potential scan rate applied at the Pt/Vulcan generator in potentiodynamic experiments was 10 mV/s.

The electrolyte flow (flow rate ca. 4 $\mu\text{l/s}$) was driven by the hydrostatic pressure of the electrolyte in the supply bottle. The supporting electrolyte (0.5 M sulfuric acid) was prepared using Millipore Q water and ultrapure sulfuric acid (Merck, suprapur), and purged by high purity Ar (MTI Gase, N 6.0) or saturated with O_2 (MTI Gase, N 5.7) in the electrolyte supply bottle. The collection efficiency of the set-up was calibrated using a $\text{Fe}^{3+}/\text{Fe}^{2+}$ redox couple in support-

ing electrolyte containing 1 mM $\text{K}_3[\text{Fe}(\text{CN})_6]$ (Merck, p.a.). All measurements were conducted at room temperature.

3. Results and discussion

3.1. Electrode characterization and calibration of the set-up versus a $\text{Fe}(\text{III})/\text{Fe}(\text{II})$ redox couple

First both electrodes were characterized by cyclic voltammetry (CV) in 0.5 M H_2SO_4 solution. A representative CV of the thin-film Pt/Vulcan electrode, which is mounted in the first compartment of the dual thin-layer flow cell, is shown in Fig. 2a (solid line). It agrees well with those reported in the literature (see, e.g. [29,30]). Assuming a density of Pt surface atoms of 1.3×10^{15} per cm^2 , a hydrogen adsorption charge for polycrystalline Pt of 0.21 mC/cm^2 [31], and a coverage of H_{ad} at the onset of bulk hydrogen evolution at 0.06 V (RHE) of 0.77 ML [32], we calculate a real (active) Pt surface area of 7 cm^2 from the hydrogen adsorption charge on the Pt nanoparticle surface (1.14 mC), after subtracting the double-layer charging current. (Note that the double layer

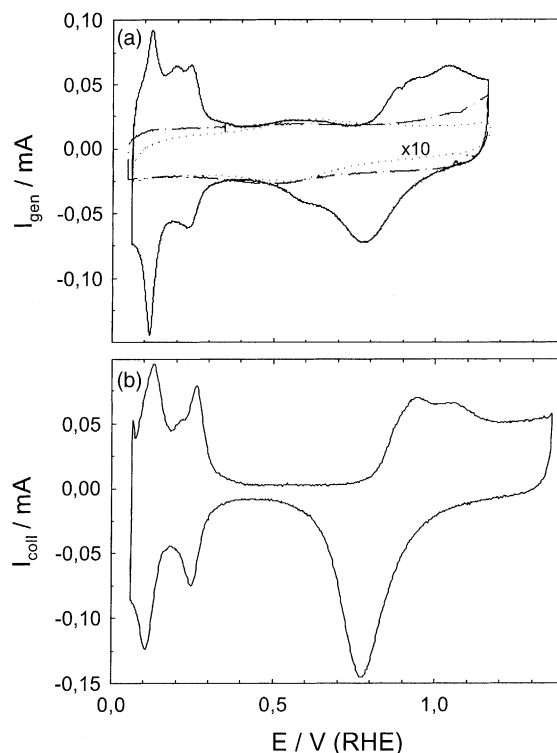


Fig. 2. Cyclic voltammograms recorded separately on a thin-film Pt/Vulcan electrode (20 wt.% Pt, Pt loading 28 $\mu\text{g/cm}^2$) (Fig. 2a, solid line), on a disperse Vulcan XC72 support electrode with similar carbon loading (loading 112 $\mu\text{g/cm}^2$) (Fig. 2a, dash-dotted line) and on a bare glassy carbon stub (Fig. 2a, dotted line, 10-fold magnified) in the first compartment of the dual thin-layer flow cell ($v = 10$ mV/s), and on a polycrystalline Pt electrode (1.33 cm^2 accessible surface area) in the second compartment of the flow cell (Fig. 2b) (scan rate $v = 50$ mV/s, Ar-saturated 0.5 M H_2SO_4 solution, electrolyte flow rate ca. 4 $\mu\text{l/s}$, room temperature).

charging current results mainly from the pseudocapacitive current of the carbon Vulcan support in the negative-going scan (Fig. 2, dash-dotted line)). This value agrees well with the results of our previous studies on the same catalyst [28], and is within the range of the Pt surface area of 5 cm^2 calculated from the total Pt loading in the electrocatalytic area, using the dispersion of ca. 26% (the ratio of surface atoms to the total number of the atoms) of the catalyst nanoparticles calculated from the TEM data [27,28], which suggests essentially full utilization of the Pt surface atoms. (It should be noted that the dispersion is calculated by assuming a spherical shape of the nanoparticles, which is known to be not precise [33], and a density of Pt surface atoms of $1.22 \times 10^{15} \text{ atoms/cm}^2$ [27]. The resulting deviations, however, would not significantly affect the above statement.)

The CVs of the second electrode (e.g. see Fig. 2b), a mirror-polished polycrystalline Pt disk with an exposed geometric surface area of 1.33 cm^2 , which is mounted in the second compartment of the dual thin-layer flow cell, also show good agreement with the well-known current–voltage response of clean polycrystalline Pt electrodes [34]. Applying the same procedure as described above the real surface area of this electrode was calculated to be 1.86 cm^2 , which corresponds to a roughness factor of ca. 1.4.

Finally, based on the absence of any significant distortions, the CVs presented in Fig. 2 demonstrate that the electrochemical measurements can be carried out in the DTLFC-DDE configuration without significant Ohmic drops.

For the quantitative determination of the electro-active species produced during a continuous (bulk) electrochemical reaction on the first electrode (generator), the collection efficiency of the second electrode (collector) has to be calibrated, similar to RRDE measurements. This was done using the Fe(III)/Fe(II) redox process, comparing the amount of Fe(II) formation in the first electrode with that of Fe(II) oxidation on the second electrode. Fig. 3a shows the CV of the Pt/Vulcan electrode in $1 \text{ mM K}_3[\text{Fe}(\text{CN})_6]$ containing $0.5 \text{ M H}_2\text{SO}_4$ solution. The broad feature in the current response to the potential of the Pt/Vulcan electrode (Fig. 3a, solid line) for ferrocyanide reduction is due to large pseudo-capacitive double-layer charging currents characteristic for Pt/Vulcan electrodes (see Fig. 2a). Assuming a symmetric double-layer contribution (see Fig. 2a, dash-dotted line), the latter can be subtracted by simply averaging the currents in the negative-going and positive-going scans. The resulting curve (Fig. 3a, dotted line) shows a mass transport limited current of ca. -0.05 mA for Fe(III) reduction to Fe(II), which is reached at potentials negative of $0.6 \text{ V}_{\text{RHE}}$. The current measured simultaneously at the polycrystalline Pt collector at a constant electrode potential of $1.16 \text{ V}_{\text{RHE}}$, which is sufficient for electro-oxidation of electrogenerated Fe(II) species, but not for oxygen evolution, is shown as a function of the potential of the first electrode in Fig. 3b. The Fe(II) electro-oxidation current to Fe(III) on the collector (Fig. 3b) closely follows the reduction current of Fe(III) to

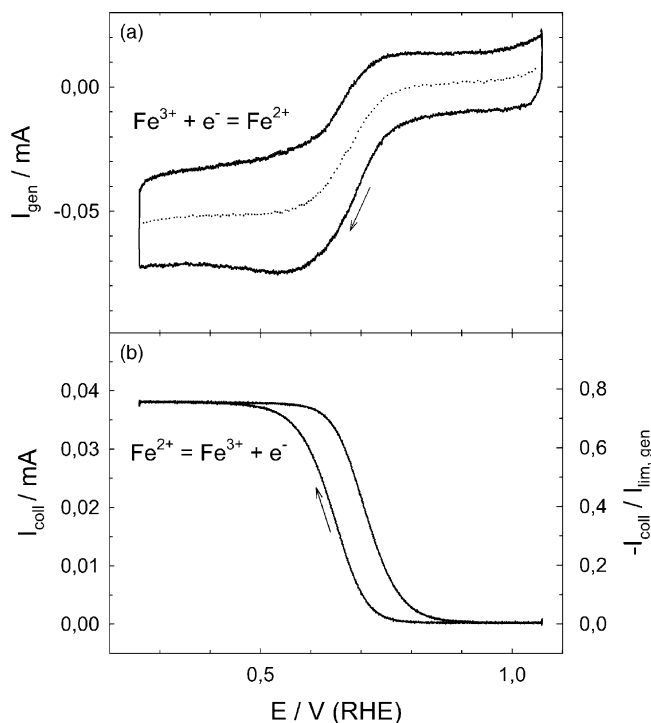


Fig. 3. Cyclic voltammogram of a thin-film Pt/Vulcan electrode (Pt loading $28 \mu\text{g/cm}^2$) in the first compartment (a), solid line) and the related current signal recorded simultaneously on a polycrystalline Pt electrode at $E = 1.16 \text{ V}$ in the second compartment (b) of a dual thin-layer flow cell in Ar-saturated $0.5 \text{ M H}_2\text{SO}_4$ solution containing $1 \text{ mM K}_3[\text{Fe}(\text{CN})_6]$ (electrolyte flow rate ca. $4 \mu\text{l/s}$, potential scan rate 10 mV/s , room temperature). The dotted line in (a) indicates the double-layer charging corrected signal, obtained by averaging the positive-going and negative-going scan of the CV. The right-hand axis in (b) indicates the collection efficiency.

Fe(II) on the generator (Fig. 3a, dotted line). The hysteresis in the negative- and positive-going scans reflects the time required for transferring the species generated at the first electrode to the second electrode (about 3 s). A constant, mass-transport-limited current of ca. 0.038 mA is obtained on the collector at generator potentials negative of $0.5 \text{ V}_{\text{RHE}}$ (Fig. 3b).

To avoid the significant pseudo-capacitive contributions encountered on the Pt/Vulcan electrode in potentiodynamic experiments (Fig. 3a), we also performed measurements at a constant potential for ferrocyanide reduction on the generator. In these experiments the generator potential was stepped from 0.96 to $0.46 \text{ V}_{\text{RHE}}$, while the collector potential was kept constant at $1.16 \text{ V}_{\text{RHE}}$ (Fig. 4). After the initial overshoot in the Faradaic current, which is at least largely due to double-layer charging upon stepping the electrode potential, the current drops to a nearly constant value of -0.05 mA (Fig. 4a), which is purely mass-transport limited. This value for ferrocyanide reduction is equal to that estimated from the CV data in Fig. 3a. The current on the collector increases accordingly after the potential step, reaching a mass transport limited value of 0.038 mA after about 5 s (ca. 90% after 3 s) (Fig. 4b). Also this value agrees well with the potentiodynamic data in Fig. 3b.

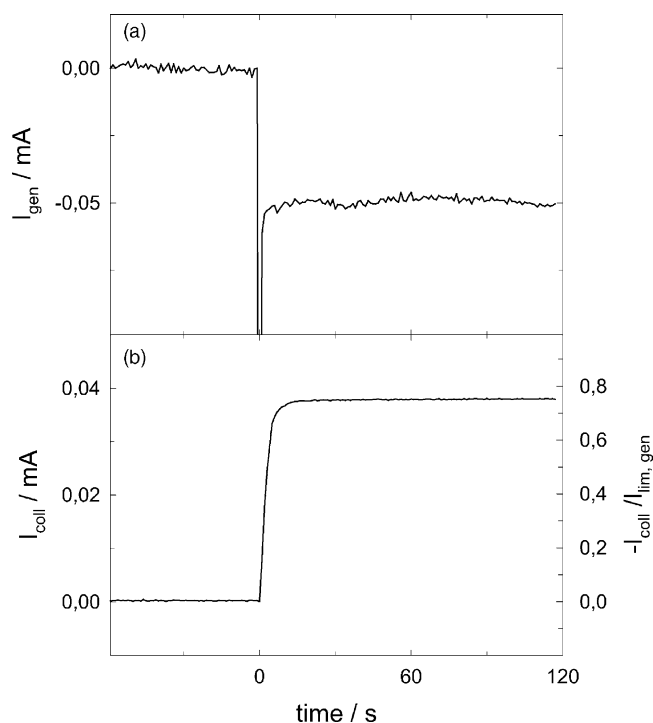


Fig. 4. Simultaneously recorded current transients upon a potential step ($0.96 \rightarrow 0.46 \text{ V}$) of the Pt/Vulcan (Pt loading $28 \mu\text{g}/\text{cm}^2$) electrode in the first compartment. (a) current on the Pt/Vulcan working electrode and (b) on the polycrystalline Pt electrode at $E = 1.16 \text{ V}$ in the second compartment of a dual thin-layer flow cell in Ar-saturated $0.5 \text{ M H}_2\text{SO}_4$ solution containing $1 \text{ mM K}_3[\text{Fe}(\text{CN})_6]$ (electrolyte flow rate ca. $4 \mu\text{l}/\text{s}$, room temperature). The right-hand axis in (b) indicates the collection efficiency.

Following Weber and Long [26] the mass-transport-limited current I_{lim} in a thin-layer channel flow cell is given by

$$I_{\text{lim}} = k \cdot n \cdot F \cdot c \cdot u^{1/3} \left(\frac{D \cdot A}{b} \right)^{2/3} \quad (1)$$

where k is the cell constant ($k = 1.467$ for a channel-flow thin-layer cell), n is the number of electrons, F is the Faraday constant, c is the concentration of the species involved in the electrochemical reaction, u is the electrolyte flow rate, D is the diffusion coefficient of the reacting species, A is the electrode surface area, and b is the thickness of the thin-layer gap, respectively. A linear dependence of the rates for ferrocyanide reduction and ferricyanide oxidation on $u^{1/3}$ was indeed found in earlier experiments on a polycrystalline Pt electrode in the first thin-layer compartment [35], which suggests that a laminar flow regime is attained in the thin layer of electrolyte at the electrode surface.

Inserting the corresponding values of $k = 1.467$, $n = 1$, $F = 96,480 \text{ A s/mol}$, $c = 1 \times 10^{-3} \text{ mol}/\text{cm}^3$, $u = 3 \times 10^{-3} \text{ cm}^3/\text{s}$, $D = 7.7 \times 10^{-5} \text{ cm}^2/\text{s}$ [36], $A = 0.28 \text{ cm}^2$ and $b = 40 \times 10^{-3} \text{ cm}$, the mass-transport-limited current for ferrocyanide reduction can be calculated to be ca. -0.1 mA according to Eq. (1). This value is about twice of that determined experimentally for ferrocyanide reduction (Figs. 3a and 4a) The deviation can be rationalized taking into account

a non-ideal flux of electrolyte over the electrode surface in our thin-layer cell, as described before in Section 2. Though a channel-flow from the inlet to each of the four connecting capillaries is achieved, stagnation regions can occur between the connecting capillaries, especially at the periphery of the electrode, so that a uniform, radial flow cannot be attained in our design. Because of the reduced flow in the stagnation regions the experimental value of the mass-transport-limited current is lower than that predicted theoretically according to Eq. (1), which assumes a uniform flux of the reactant over the whole electrode surface. This situation can be partly improved increasing the number of the connecting capillaries [37], which, however, causes an increase in the total volume and hence in the time constant of the cell. For a more detailed description of the electrolyte flow in thin-layer channel electrochemical reactors see [22,38] and references cited therein.

Similar to the definition for the RRDE configuration [5] the collection efficiency N for a one-electron electrochemical reaction is given by the ratio of the collector current to the (mass-transport-limited) current at the generator,

$$N = \frac{-I_{\text{coll}}}{I_{\text{lim,gen}}} \quad (2)$$

From the data of Figs. 3 and 4 the collection efficiency for the dual thin-layer cell double-disk electrode set-up is 0.76 (or 76%). This value is about four-fold higher than that of a typical RRDE configuration (typically ca. 20%, depending on the design dimensions of the ring-disk electrode [5]), and about similar to those reported for a radial thin-layer ring-disk configuration [23,39] or a dual-band electrode configuration [22]. Due to the large area of the collector our double-disk electrode approach achieves a high collection efficiency at a time constant of ca. 3 s, and, therefore, is advantageous compared to both an RRDE set-up or a thin-layer ring-disk/dual band electrode configuration for sensing small amounts of electro-active species generated at the working electrode, such as peroxide in the oxygen reduction reaction, at moderate potential scan rates ($10 \text{ mV}/\text{s}$ or below), as will be demonstrated later in Section 3.2. The proposed DTLFC-DDE configuration can hardly be used, however, for the detection of short-lived intermediates. In such cases an RRDE configuration, with the almost instantaneous detection at the ring, would be the suitable instrument.

3.2. Oxygen reduction reaction studied in the dual thin-layer double-disk electrode set-up

For demonstrating the performance of the DTLFC-DDE set-up, we present measurements of the oxygen reduction reaction (ORR) on a Pt/Vulcan electrode (Fig. 5a), where we detect simultaneously the hydrogen peroxide oxidation on the polycrystalline Pt collector at 1.16 V (Fig. 5b), which allows us to evaluate the peroxide yields as a function of the electrode potential. This reaction had been studied in our group on the same catalyst in thin-film RRDE measurements previously [40].

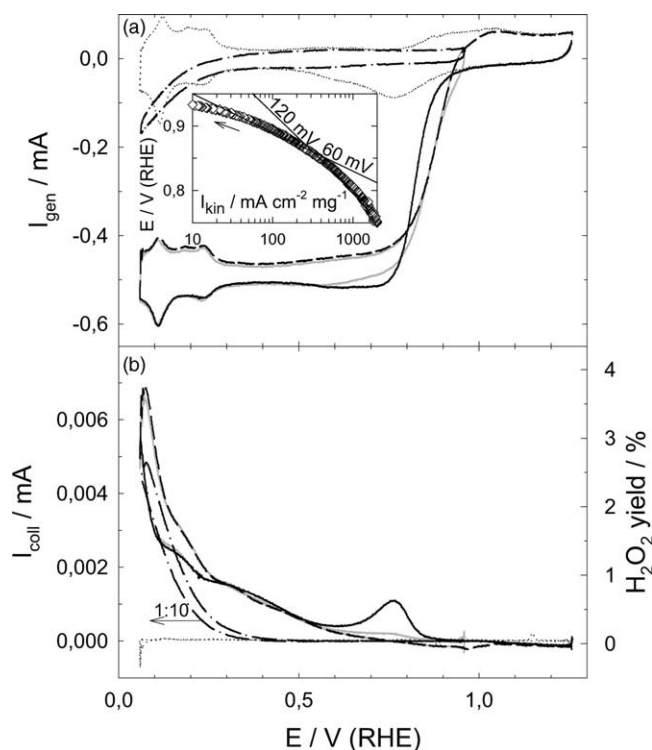


Fig. 5. Simultaneously recorded cyclic voltammograms of a Pt/Vulcan electrode (Pt loading $28 \mu\text{g}/\text{cm}^2$) and of a Vulcan carbon electrode (loading $112 \mu\text{g}/\text{cm}^2$) in the first compartment (a), and the related current signals recorded simultaneously on a polycrystalline Pt electrode at $E = 1.16 \text{ V}$ in the second compartment (b) of a dual thin-layer flow cell. The right-hand axis in (b) indicates the peroxide yield on the Pt/Vulcan electrode. Dotted line: base voltammogram of the Pt/Vulcan electrode in Ar-purged $0.5 \text{ M H}_2\text{SO}_4$ solution; dashed line, full line: voltammogram of the Pt/Vulcan electrode in O_2 -saturated $0.5 \text{ M H}_2\text{SO}_4$ solution (positive-going scan: dashed line, negative-going scan: full line), gray line: similar CV with a positive potential limit of 0.96 V ; and dash-dotted line: voltammogram of the Vulcan carbon electrode in O_2 -saturated $0.5 \text{ M H}_2\text{SO}_4$ solution: (electrolyte flow rate ca. $4 \mu\text{l}/\text{s}$, potential scan rate $10 \text{ mV}/\text{s}$, room temperature). Inset Fig. 5a: Tafel plot for the ORR current during the positive-going scan.

The CV recorded on the Pt/Vulcan catalyst in O_2 saturated solution (Fig. 5a, full line, dashed lines) largely resembles the base CV in sulfuric acid (Fig. 5a, dotted line) plus a superimposed O_2 reduction current, which is transport limited to ca. -0.5 mA in the potential region negative of the formation/reduction of PtO. The theoretical value for the mass-transport-limited current, calculated according to Eq. (1) for channel-flow with an electron number of $n = 4$, a diffusion coefficient for O_2 diffusion of $D = 1.93 \times 10^{-5} \text{ cm}^2/\text{s}$, and an O_2 concentration in the O_2 saturated solution of $c = 1.26 \times 10^{-6} \text{ mol}/\text{cm}^3$ [41], is ca. -1.2 mA . Again the difference to the lower experimental value is explained by a non-ideal flux of the electrolyte at the electrode, as discussed in Section 3.1. It is important that the difference between the theoretical and experimental value for the transport-limited current for O_2 reduction is the same as that found for ferrocyanide reduction, suggesting the same transfer characteristics. Therefore the collection efficiency found

for ferrocyanide reduction reaction can be used also for the quantitative evaluation of the O_2 reduction pathways.

The turnover frequency or TOF number, defined as the number of O_2 molecules reduced per Pt surface atom and per second, can be calculated from

$$\text{TOF} = \left(\frac{-i}{nF} \right) \frac{N_A}{N_s} \quad (3)$$

where i is the oxygen reduction current, n is the number of electrons (4 for O_2 reduction to water), F is the Faraday constant, N_A the Avogadro number (6.02×10^{23} molecules/mol), and N_s is the number of Pt surface atoms (1.3×10^{15} atoms/ cm^2 , multiplied by the real Pt surface area of the catalyst, as derived found from hydrogen UPD on the Pt/Vulcan electrode, see Section 3.1.). The mass-transport-limited current of ca. -0.5 mA corresponds to a turn over frequency of about 0.07 molecules site $^{-1}$ s $^{-1}$. Note that at the higher flux in a typical RRDE measurement considerably higher values are obtained for the mass-transport-limited current and the corresponding TOF values (The ca. $-1.5 \text{ mA}/\text{cm}^2$ of geometric area obtained here correspond roughly to that found for a rotation rate of 100 rpm in an RRDE configuration [40]).

The hysteresis between the negative-going (Fig. 5a, solid line) and positive-going (Fig. 5a, dashed line) scan in the potential region 0.8 – 1.0 V is generally explained by the quasi-reversible formation/reduction of PtO, (see, e.g. [42]). At a positive potential limit of 0.96 V (Fig. 5a, gray line) it follows the ORR in the positive-going scan (Fig. 5a, dashed line), indicating that under these conditions PtO formation is negligible. The inset in Fig. 5a shows a Tafel plot of the kinetic O_2 reduction current (defined as $I_{\text{kin}} = I_{\text{lim}} \times I / (I_{\text{lim}} - I)$ per one milligram of the catalyst [43] in the region 0.75 – 0.95 V during the positive-potential scan, which is in good agreement with that reported previously in RRDE measurements [40], despite the lower value of the mass-transport-limited current obtained under present conditions in the DTLFC-DDE configuration. The slope of approximately 60 mV per decade in the close-to-linear part of the kinetic ORR current in the “low-current” region ($E > 0.87 \text{ V}$), which is usually interpreted as evidence of a first single-electron transfer to the adsorbed O_2 as the rate-determining step [44], and the transition to a ca. 120 mV per decade slope in the “high current” region ($E < 0.87$) agree well with the literature data for the ORR in an R(R)DE configuration on polycrystalline [45], single-crystal [46] and nanoparticle [40,47] Pt electrodes.

Fig. 5b shows the current measured on the collector at 1.16 V in parallel to the cyclic voltammograms plotted in Fig. 5a. The collector signal is essentially zero over the entire potential range for the base CV in Ar-saturated 0.5 M sulfuric acid solution (dotted lines in Fig. 5). In O_2 -saturated $0.5 \text{ M H}_2\text{SO}_4$ solution the collector current increases significantly at potentials negative of 0.6 V for the positive potential limit of 0.96 V (Fig. 5b, gray line). Qualitatively, the current at the collector follows the well-known peroxide formation

features found at the ring electrode during the ORR on polycrystalline Pt and Pt/Vulcan electrodes in RRDE measurements [40,47,48]. The maximum currents reached on the collector at 0.06 V are similar to those measured on the ring in a RRDE configuration at rotation rates of 1600 rpm, though the O₂ reduction current on the generator in our configuration is only about one-third of that on the RRDE disk. This underlines the high sensitivity and excellent signal-to-noise ratio of the DTLFC-DDE set-up for peroxide detection due to the ca. 4-fold higher collection efficiency than in a standard RRDE set-up (see Section 3.1).

The hydrogen peroxide yield in the ORR, $X(\text{H}_2\text{O}_2)$, is quantified via [40]

$$X(\text{H}_2\text{O}_2) = \frac{(2 \times I_{\text{coll}}/N)}{(I_{\text{gen}} + I_{\text{coll}}/N)}, \quad (4)$$

where I_{coll} and I_{gen} are the currents on the collector and generator, respectively, and N is the collection efficiency determined for ferrocyanide reduction ($N = 0.76$, see Section 3.1) (the resulting value is multiplied by 100 for the yield in percentage). The corresponding scale on the right-hand axis of Fig. 5b shows that the maximum peroxide formation yield achieved at 0.06 V is about 4%. This value is in an excellent agreement with the 5–6% peroxide yields at this potential detected on the same Pt/Vulcan catalyst in RRDE measurements (at 1600 rpm and 60 °C), taking into account that part of the peroxide formed on the Pt/Vulcan electrode can be decomposed during the transfer to the collector (ca. 3 s) in our set-up, while in the standard RRDE configuration the transport times are much smaller and the peroxide detection is almost instantaneous.

Since O₂ is known to be reduced mainly to peroxide on carbon at potentials negative of 0.3 V [40,49], we also performed test experiments on a Pt-free Vulcan thin-film electrode (Fig. 5, dash-dotted lines). The CV of the Vulcan thin-film electrode shows an exponentially increasing oxygen reduction current at potentials negative of 0.4 V (Fig. 5a, dash-dotted line), along with a simultaneous increase in peroxide formation (Fig. 5b, dash-dotted line). Note that the peroxide formation current at the negative potential limit (0.06 V) on Vulcan carbon is ca. 7 times higher (scaled down by one order of magnitude in Fig. 5b) compared to that on the Pt/Vulcan catalyst (Fig. 5b, full line/dashed line), even though the oxygen reduction current on Vulcan is only about one third of that (Fig. 5a). This suggests a high current efficiency for oxygen reduction to peroxide on Vulcan carbon (ca. 50%, according to Eq. (4)), in agreement with previous RRDE data [50]. In the presence of catalytically active Pt nanoparticles on the Vulcan carbon support, however, the ORR proceeds preferably via the four electron pathway (on Pt), resulting in a decrease in peroxide yield by 90% compared to Vulcan carbon (Fig. 5b). Assuming that on Pt/Vulcan the ORR occurs on both carbon and Pt and that both reaction channels contribute to peroxide formation, this indicates that part of the H₂O₂ formed on the carbon support is further reduced to water (or decom-

posed) on the Pt nanoparticles. These additional side reactions complicate a direct comparison of the catalytic activity of carbon-supported fuel cell catalysts and massive noble metal model electrodes surfaces with respect to peroxide formation.

To better separate the complex features in peroxide formation rate as a function of the electrode potential occurring in potentiodynamic experiments (Fig. 5b) and to determine the time resolution of the DTLFC-DDE set-up in experiments involving a change in electrolyte, we performed transient measurements of the ORR on Pt/Vulcan and Vulcan carbon thin-film electrodes at a constant electrode potential (0.06 V), switching from a (stagnant) Ar-saturated 0.5 M sulfuric acid electrolyte to an O₂-saturated 0.5 M sulfuric acid electrolyte flow (Fig. 6). On both electrodes, the ORR currents attain constant, mass-transport-limited values ca. 5 s after the O₂-saturated electrolyte starts to reach the respective electrodes (90% of the limiting value in ca. 2 s) (Fig. 6a). These time constants reflect the time required to completely replace the electrolyte film on the electrode by O₂-containing solution. In order to better illustrate the time resolution we also show the signal for the Pt/Vulcan electrode on a 10-fold

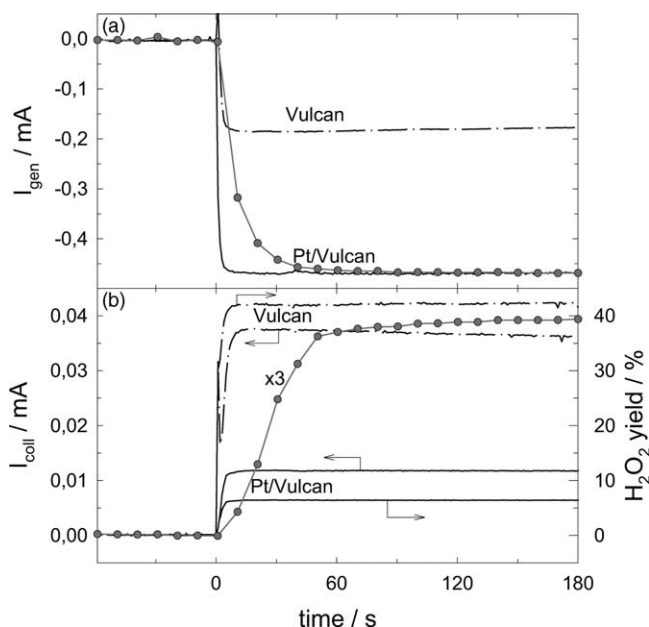


Fig. 6. Current transients recorded simultaneously after starting to flow O₂-saturated electrolyte through the flow cell on the Pt/Vulcan electrode ((a), solid black line) (Pt loading 28 μg/cm²) and on a Vulcan carbon electrode ((a), dash-dotted black line) (loading 112 μg/cm²) at $E = 0.06$ V in the first compartment, and on a polycrystalline Pt electrode ((b), corresponding solid lines) at $E = 1.16$ V in the second compartment of a dual thin-layer flow cell (electrolyte flow rate ca. 4 μl/s, room temperature). The right-hand axis in (b) corresponds to the peroxide yields on the Pt/Vulcan and carbon Vulcan electrodes, respectively. The initial response of the current signal on the Pt/Vulcan electrode is more clearly resolved on a tenfold magnified time scale (full gray lines marked with dots which represent the individual measurements at the acquisition rate of one point per second). For better comparison with the electrochemical current signal on Pt/Vulcan in Fig. 6a (gray line) the collector current in Fig. 5b (gray line) is multiplied by a factor of 3.

expanded time scale (gray line with dots). The dots indicate the individual measurements at an acquisition rate of one point per second. The collector current is in addition multiplied by a factor of three to obtain signals of similar magnitude in Fig. 6a and b. The difference in the time response between the two signals, i.e., the smoother increase of the signal in Fig. 6b, reflects the additional smear out occurring during the electrolyte transport from the first to the second compartment. Likewise, the larger time constant in this experiment compared to that in the potential jump experiment can be explained by the time required to build up a constant flow situation at the Pt/Vulcan electrode after opening the electrolyte valve, while in the latter case the potential jump occurs under constant flow conditions and the time resolution is determined only by the transfer of reactive species to the collector. (The response time of the potential is much lower than that for reaching steady-state flow conditions.)

The ORR current on the Vulcan carbon electrode (Fig. 6a, dash-dotted line) is ca. 2.5 times lower than that on Pt/Vulcan (Fig. 6a, black line). On the other hand, the hydrogen peroxide oxidation current on the Vulcan carbon electrode (Fig. 6b, dash-dotted line) is about 3 times higher than that on the Pt/Vulcan electrode (Fig. 6b, black line). In combination, these two results suggest different reaction pathways on both electrodes. The peroxide yields obtained at 0.06 V on the respective generator electrodes (Fig. 6b), which are calculated according to Eq. (4), are about 6.5% on the Pt/Vulcan electrode (black line) and 42.5% on the Vulcan carbon electrode (dash-dotted line), respectively. The slightly different values for peroxide yields derived in the potentiodynamic measurements on the two electrodes (Fig. 5) most likely result from both the time delay in peroxide detection and pseudo-capacitive contributions.

Overall, the potentiostatic measurements demonstrate that the time resolution of the DTLFC-DDE set-up is sufficient for performing transient kinetic measurements which involve electrolyte exchange. In combination with the high collection efficiency this method is therefore particularly suitable for mechanistic and kinetic studies of electrocatalytic reactions where electrolyte exchange is mandatory. A typical example is the study of the chemical CO oxidation by O₂ in the anode of a polymer electrolyte fuel cell (PEFC) and the simultaneous ORR on CO_{ad}-covered anode catalysts, which is highly interesting for the understanding of the reactions going on during 'air-bleed' operation of PEFCs (see [25,51]).

4. Summary

We have presented a novel double-disk electrode design, which is based on a dual thin-layer flow cell. Due to its high collection efficiency in combination with a reasonable time resolution it allows the highly sensitive determination of electro-active species generated during electrocatalytic reactions on the working electrode. Under present continuous

flow conditions electro-active species formed at the generator are detected at the potential-controlled collector with a delay of ca. 3 s and a collection efficiency of 76%. Using thin-film electrodes it allows time-resolved studies of electrocatalytic reactions on supported catalysts or model catalysts, including single-crystal electrodes, under defined electrolyte flow conditions, which makes it particularly attractive for model studies on fuel cell reactions under realistic conditions (continuous reaction, continuous electrolyte flow) and on realistic materials (supported catalysts) under nevertheless well-defined conditions. Most important, and its main advantage in comparison to the commonly used RRDE configuration, however, is its ability to quickly exchange the electrolyte during measurements, which allows kinetic studies of electrocatalytic reactions that require a change in electrolyte. The time resolution in transient experiments involving a change in electrolyte, defined by the time required to reach 90% of the final signal, is about 2 s.

The performance of this set-up is tested in potentiodynamic and potentiostatic measurements of the ORR on supported Pt/Vulcan catalysts and, for comparison, on Pt-free Vulcan carbon support. The good agreement with existing RRDE data demonstrates the general suitability of the set-up. The higher sensitivity allowed to clearly identify a maximum around 0.78 V in the collector current in the negative-going scan of a CV in O₂-containing electrolyte, which is attributed to H₂O₂ formation on partly oxide covered Pt catalyst under these conditions. The significantly higher rate for H₂O₂ formation at potentials negative of 0.3 V, with a H₂O₂ formation yield of more than 40% on Pt-free Vulcan carbon, compared to that on the Pt/Vulcan catalyst indicates that on the latter catalyst part of the H₂O₂ formed on the carbon support is further reduced to H₂O or decomposed. Transient experiments changing from an Ar-saturated electrolyte to a flow of O₂-saturated electrolyte under potential conditions, where the electrodes are active for O₂ reduction and H₂O₂ oxidation, respectively, illustrate the time resolution of the set-up and its suitability for transient kinetic studies of such type.

Acknowledgements

We gratefully acknowledge financial support by the state of Baden-Württemberg, within the 'Zukunftsoffensive Junge Generation', by the Federal Ministry of Education, Research and Technology (BMBF, Grant 01SF0053) and by the Deutsche Forschungsgemeinschaft (Be 1201/8-4).

References

- [1] V.G. Levich, *Physicochemical Hydrodynamics*, Prentice Hall, Englewood Cliffs, NJ, 1962.
- [2] T.J. Schmidt, H.A. Gasteiger, in: W. Vielstich, A. Lamm, and H.A. Gasteiger (Eds.), *Handbook of Fuel Cells—Fundamentals*

- Technology and Applications, Vol. 2. Electrocatalysis, John Wiley & Sons, New York, 2003, p. 316.
- [3] N.M. Markovic, in: W. Vielstich, A. Lamm, H.A. Gasteiger (Eds.), *Handbook of Fuel Cells—Fundamentals Technology and Applications*, Vol. 2. Electrocatalysis, John Wiley & Sons, New York, 2003, p. 368.
- [4] P.N. Ross, in: W. Vielstich, A. Lamm, and H. A. Gasteiger (Eds.), *Handbook of Fuel Cells—Fundamentals Technology and Applications*, Vol. 2. Electrocatalysis, John Wiley & Sons, New York, 2003, p. 465.
- [5] W.J. Albery, M.L. Hitchman, *Ring-Disc Electrodes*, Clarendon Press, Oxford, 1971.
- [6] A.N. Frumkin, L. Nekrasov, V.G. Levich, J. Ivanov, *J. Electroanal. Chem.* 1 (1953) 84.
- [7] J. Yamada, H. Matsuda, *J. Electroanal. Chem.* 44 (1973) 189.
- [8] W.J. Albery, *J. Electroanal. Chem.* 191 (1985) 1.
- [9] P. Laevers, A. Hubin, H. Teryn, J. Vereeken, *J. Appl. Electrochem.* 25 (1995) 1017.
- [10] W.J. Albery, C.C. Jones, A.R. Mount, in: R.G. Compton, A. Hamnett (Eds.), *Chemical Kinetics*, Vol. 29, Elsevier Publications, Amsterdam, 1986.
- [11] C.M.A. Brett, A.M.F.C. Oliveira Brett, in: C.H. Bamford, R.G. Compton (Eds.), *Chemical Kinetics*, Vol. 26, Elsevier Publications, Amsterdam, 1986.
- [12] P.R. Unwin, R.G. Compton, in: C.H. Bamford, R.G. Compton (Eds.), *Chemical Kinetics*, Vol. 26, Elsevier Publications, Amsterdam, 1986.
- [13] M. Bergelin, M. Wasberg, *J. Electroanal. Chem.* 449 (1998) 181.
- [14] M. Bergelin, J.M. Feliu, M. Wasberg, *Electrochim. Acta* 44 (1998) 1069.
- [15] M. Bergelin, E. Herrero, J.M. Feliu, M. Wasberg, *J. Electroanal. Chem.* 467 (1999) 74.
- [16] U. Koponen, T. Peltonen, M. Bergelin, T. Mennola, M. Valkiainen, J. Kaskimies, M. Wasberg, *J. Power Sources* 86 (2000) 261.
- [17] T.H. Madden, N. Arvindan, E.M. Stuve, *J. Electrochem. Soc.* 150 (2003) E1.
- [18] N. Wakabayashi, H. Uchida, M. Watanabe, *Electrochem. Solid State Lett.* 5 (2002) E62.
- [19] H. Gerischer, I. Mattes, R. Braun, *J. Electroanal. Chem.* 10 (1965) 553.
- [20] W.J. Albery, C.M.A. Brett, *J. Electroanal. Chem.* 148 (1983) 201.
- [21] R.G. Compton, A.C. Fisher, M.H. Latham, C.M.A. Brett, A.M.C.F. Oliveria Brett, *J. Appl. Electrochem.* 22 (1992) 1011.
- [22] A. Paixaoa, R.C. Matos, M. Bertotti, *Electrochim. Acta* 48 (2003) 691.
- [23] K. Toda, S. Oguni, Y. Takamatsu, I. Sanemasa, *J. Electroanal. Chem.* 479 (1999) 57.
- [24] Z. Jusys, H. Massong, H. Baltruschat, *J. Electrochem. Soc.* 146 (1999) 1093.
- [25] Z. Jusys, J. Kaiser, R. J. Behm, *J. Electroanal. Chem.* 554/555 (2003) 427.
- [26] S.G. Weber, J.T. Long, *Anal. Chem.* 60 (1988) 903A.
- [27] T.J. Schmidt, H.A. Gasteiger, G.D. Stäb, P.M. Urban, D.M. Kolb, R.J. Behm, *J. Electrochem. Soc.* 145 (1998) 2354.
- [28] Z. Jusys, J. Kaiser, R.J. Behm, *Langmuir* 19 (2003) 6759.
- [29] T.J. Schmidt, H.A. Gasteiger, R.J. Behm, *J. Electrochem. Soc.* 146 (1999) 1296.
- [30] B. Rush, J.A. Reimer, E.J. Cairns, *J. Electrochem. Soc.* 148 (2001) A137.
- [31] V.S. Bagotzky, Y.B. Vassilyev, *Electrochim. Acta* 12 (1967) 1323.
- [32] T. Biegler, D.A.J. Rand, R. Woods, *J. Electroanal. Chem.* 29 (1971) 269.
- [33] A.I. Frenkel, C.W. Hills, R.G. Nuzzo, *J. Phys. Chem. B* 105 (1997) 12689.
- [34] H. Angerstein-Kozłowska, B.E. Conway, W.B.A. Sharp, *J. Electroanal. Chem.* 43 (1973) 9.
- [35] Z. Jusys, H. Baltruschat, unpublished.
- [36] P. Laevers, A. Hubin, H. Teryn, J. Vereeken, *J. Appl. Electrochem.* 25 (1995) 1023.
- [37] H. Wang, T. Löffler, H. Baltruschat, *J. Appl. Electrochem.* 30 (2001) 759.
- [38] I.E. Henley, K. Yunus, A.C. Fisher, *J. Phys. Chem. B* 107 (2003) 3878.
- [39] B. Soucaze-Guillous, W. Kutner, *Electroanalysis* 9 (1997) 32.
- [40] U.A. Paulus, T.J. Schmidt, H.A. Gasteiger, R.J. Behm, *J. Electrochem. Soc.* 495 (2001) 134.
- [41] N.M. Markovic, H.A. Gasteiger, P.N. Ross, *J. Phys. Chem.* 99 (1995) 3411.
- [42] S. Gottesfeld, I.D. Raistrick, S. Srinivasan, *J. Electrochem. Soc.* 134 (1987) 1455.
- [43] S.L. Gojkovic, S.K. Zecevic, R.F. Savinell, *J. Electrochem. Soc.* 145 (1998) 3713.
- [44] M.R. Tarasevich, A. Sadkowski, E. Yeager, in: J.O.M. Bockris et al. (Eds.), *Comprehensive Treatise in Electrochemistry*, Plenum Press, New York, 1983.
- [45] A. Damjanovic, M.A. Genshaw, J.O. Bockris, *J. Electrochem. Soc.* 114 (1967) 466.
- [46] N. Markovic, H.A. Gasteiger, P.N. Ross, *J. Electrochem. Soc.* 144 (1997) 1591.
- [47] U.A. Paulus, A. Wokaun, G.G. Scherer, T.J. Schmidt, V. Stamenkovic, V. Radmilovic, N.M. Markovic, P.N. Ross Jr, *J. Phys. Chem. B* 106 (2002) 4181.
- [48] T.J. Schmidt, U.A. Paulus, H.A. Gasteiger, R.J. Behm, *J. Electroanal. Chem.* 508 (2001) 41.
- [49] K. Kinoshita, *Electrochemical Oxygen Technology*, John Wiley & Sons, New York, 1992.
- [50] U.A. Paulus, Diploma Thesis, University of Ulm, 1998.
- [51] Z. Jusys, J. Kaiser, R.J. Behm, submitted for publication.